Chapter 4

Natural Frequency Estimator

A parameter estimator is required to form an adaptive control method. In this chapter, a new method for estimating the natural frequency of a flexible structure is presented. The chapter starts with a review of the various methods for estimating the natural frequency of a system, along with their shortcomings. This is followed by a description of the proposed method. A brief discussion of the general concept of on-line parameter estimation, and a review of the standard RLS algorithm are given in Section 4.2. Stability analysis and an analysis of the factors that influence the accuracy of RLS are given in Sections 4.3 and 4.4, respectively. The proposed natural frequency estimator method is then given in Section 4.5. The results from the simulation studies and the experimental implementation to evaluate the performance of the proposed method are presented in Sections 4.6 and 4.7, respectively.

4.1 Introduction

As can be seen from Chapter 3, the M^{4}RC method is capable of effectively controlling a vibrating system with varying loads if all the possible loading conditions are *a priori* known. If, however, the loading conditions cannot be previously predicted (e.g., when the damage to an aircraft wing changes its loading or damping properties, or when a robot arm is lifting samples of unknown mass and/or is

being subjected to unforeseen disturbances), then an adaptive resonant control method is required to handle such variability, which goes beyond the control capability of its fixed-parameter multiple-model counterpart.

In an adaptive control method, the plant parameters are identified on-line at every instant and the controller parameters are updated in response to variations of the plant parameters. This adaptation of the parameters enables the controller to achieve optimum attenuation during load variations.

Three parameters (i.e., controller gain, damping ratio and centre frequency) are involved in the resonant control design, as can be seen in (3.3). To implement an efficient and effective adaptive resonant controller, an analysis to determine which parameter(s) need to be updated is required. The analysis takes into account the amount of computation needed to update the controller parameters, and the sensitivity of the controller's attenuation performance to variations of the plant parameters.

To achieve optimum attenuation, the controller centre frequency can be readily set to be the same as the natural frequency of the plant. However, there is no simple relationship between the controller gain and damping ratio with the plant parameters. Optimum values of the controller gain and damping ratio can be found through a trial and error procedure. From the relation between the controller parameters and the plant parameters, it can be seen that the amount of computation needed to calculate the controller centre frequency is much less than that needed to calculate the other controller parameters.

As can be seen from example 3.2.1 in Chapter 3, the attenuation of the resonant control is sensitive to the plant natural frequency variation and not sensitive to the plant damping ratio variation. A small discrepancy between the plant natural frequency and the controller centre frequency produces poor attenuation, while a large variation to the plant damping ratio only produces a small variation

to the attenuation. Therefore the controller centre frequency plays a major role in the determination of the controller's performance.

From this discussion, it can be concluded that effective adaptive resonant control can be obtained by setting the damping ratio and gain of the controller to fixed values, and choosing the controller centre frequency as the adjustable parameter.

Since in and adaptive resonant control method the controller centre frequency must be set to the same value as the plant natural frequency, a natural frequency estimator is required to update the controller centre frequency. In the context of adaptive control, the overall performance of the control system is significantly affected by the performance of the estimator. Therefore to obtain a high performance adaptive control, a high performance estimator is required.

To implement adaptive resonant control several requirements for the natural frequency estimator are essential. The estimator must be: on-line, accurate, multi-mode, and simple. To be able to up-date the controller centre frequency at every instant, the estimator must be able to operate on-line. Due to the sensitivity of the controller to the plant natural frequencies estimation accuracy is essential for optimum performance. Since the controller is intended to control multi-mode vibration, the estimator must be able to estimate multiple modes of natural frequency simultaneously. Finally, a feasible real-time implementation requires an estimator that uses the minimal amount of computation. An estimator with a simple algorithm is favoured for adaptive resonant control.

Several methods which can be used to estimate the natural frequencies of flexible structures can be found in the literature: modal testing [31, 140], goal programming optimisation [124], maximum likelihood [145, 146], transformation [111, 127, 155], adaptive input shaping [28], modal filter [17, 77, 78] and the combined RLS-Bairstow method [121, 122].

Modal testing is the most widely used method [31]. Modal testing is an experimental procedure in which the natural frequencies of a structure are determined by vibrating the structure with a known excitation. While it vibrates, the structure will behave in such a way that some of the frequencies will not respond at all or be highly attenuated, and some frequencies will be amplified in such a way that the only limiting factor is the energy available to sustain the vibration. These frequencies, where the structure resonates, are the natural frequencies of the structure. Stöbener and Gaul [140] used modal testing to find the modal parameters of a car body, and using the parameters they obtained they designed a modal controller to attenuate the vibration in the car body. Although the results show that modal testing is able to accurately find the natural frequencies of the structure, this method can only be applied to structures with fixed parameters. Computing the modal parameters for variable structures is computationally demanding and not feasible for on-line adaptation.

The *goal programming optimisation method* [124] and the *maximum likelihood method* [145, 146] are methods that can be used to accurately estimate modal parameters (i.e., natural frequency and damping ratio) in noisy frequency response functions (FRFs). In both methods, an initial estimation of modal parameters is used to form an estimate of FRFs. The accurate values of the modal parameters are then estimated by minimising the difference between the measured FRFs and the estimated FRFs iteratively, using the goal programming algorithm or the maximum likelihood algorithm. Both of the methods, however, can only be used off-line since they require the full set of experimentally measured FRFs as the basis for minimisation.

Transformation methods such as the Fast Fourier Transform (FFT) [155] and the Wavelet Transform (WT) [111, 127] are also used to estimate the natural frequency of a structure. In the transformation methods an excitation is applied

to vibrate a structure. The structure's output signal is then transformed into the frequency domain to obtain a frequency spectrum. The natural frequencies of the system are identified in terms of the spectrum's peak responses. One shortcoming of the transformation methods is computational complexity. The number of calculations for the Radix-2 FFT algorithm is $\frac{N}{2} \, log_2 N$ complex multiplications and $N log_2 N$ complex additions, where N is the number of samples of the signal [117]. The FFT also requires batch processing of N time samples of the signal simultaneously to produce spectrum estimates at discrete frequency spacings of N^{-1} times the sampling frequency. As an illustration, to obtain 0.5 Hz estimation accuracy using a 1 kHz sampling frequency, 2048 samples are required. For this number of samples, 11,264 complex multiplications and 22,528 complex additions need to be executed in the FFT algorithm. Therefore to estimate the natural frequencies of multiple modes with reasonable accuracy, a large computational effort is required. While the FFT computational complexity may be acceptable for some signal processing methods, it is less likely to be satisfactory for adaptive control methods, where estimates of the plant are used to tune the controller [15]. Similarly to the FFT method, the WT method is computationally complex.

The *adaptive input shaping method* (AIS) [28] is a method which can be used to estimate and track the natural frequency of a system. In this method, a learning rule based on the measurement of the phase and the vibration percentage of the residual vibration is used to estimate the natural frequency of the system. The vibration percentage is calculated by comparing the magnitude of vibration before and after the shaping process, and the phase is estimated using a least-squares method based on trigonometric identity. This method offers more efficient computation than the FFT. For N signal samples, AIS only needs $14N + 6$ real multiplications, $10N - 7$ real additions, N power calculations, $2N$ table look-ups and one division. To obtain the same accuracy as with FFT only $0.05N$ signal

samples are required with AIS [28]. As an illustration, to obtain a 0.5 Hz estimation accuracy using a 1 kHz sampling frequency, 103 samples are required. The method then needs to calculate 1448 real multiplications, 1023 real additions, 103 power calculations, 206 table look-ups and one division, around 10% of the number of computations required by the FFT. This method can be used to estimate the natural frequency of a multi-mode system by isolating each mode of interest using filters, and then applying the algorithm to the filtered responses, one algorithm for each mode. The computational load, however, will increase in proportion to the number of modes. Another limitation of this method is that the convergence of the estimation to the actual frequency is only guaranteed if the initial estimate is within the region $\pm 50\%$ of the actual frequency. Therefore for systems with large natural frequency variations, the method cannot track the variations and consequently accurate estimation cannot be obtained.

Lim *et al.* [77] used an *adaptive filter* to estimate the natural frequency of a flexible structure to detect structural damage. The adaptive filter is formed as a modal filter to represent a single-degree-of-freedom transfer function, and the coefficients of the filter are updated using the least-mean-squares algorithm. Due to the use of a modal filter, which represents a single mode system, this method is only able to estimate the natural frequency for a single mode. To enable multi-mode frequency estimation, Bosse *et al.* [17] combined the modal filter with neural networks in their endeavour to estimate the natural frequencies of a space truss structure. The neural networks updates the filter's coefficients and works as a band-pass filter to isolate any one mode from the other modes. To estimate multi-mode natural frequencies, a set of parallel combined modal filter - neural networks is used. The use of a modal filter requires one sensor for each mode of interest, which is a disadvantage. Furthermore, due to the large number of computations required, this method converges slowly. This slow convergence rate is acceptable for a space structure, but it is not suitable for structures that

have a relatively short time constant compared to that of a space structure.

Rew *et al.* [121, 122] surveyed the frequency estimation approaches and developed a real-time multi-mode natural frequency estimator based on the Recursive Least-Squares (RLS) method combined with the Bairstow method. The Bairstow method is an algorithm for finding the roots of a real polynomial of arbitrary order. Using this method an even order polynomial can be decomposed into several second-order polynomials. In the combined RLS-Bairstow method, estimation is achieved in two steps. In the first step the coefficients of the characteristic equation of the system are estimated using the RLS algorithm. The result from the estimation is a polynomial of order $2M$, where M is the number of modes of interest. In the second step, the polynomial is decomposed into M second-order polynomials. From each second-order polynomial, the natural frequency of each mode can be extracted. The RLS method is selected for this application because it gives fast parameter convergence allowing fast adaptation under changing conditions and requires a relatively small computational effort, which is crucial for real-time applications. The total number of calculations required in the RLS is only $4n^2$ where n is the order of the system [61], which is very low compared to the FFT and AIS methods. Rew *et al.* [121, 122] then used the estimator in an adaptive positive position feedback control to attenuate vibration in a wing like composite structure. The experimental results from those papers show that for multi-mode frequency estimation, the estimator is sensitive to the choice of sampling rate and to unmodeled high frequency modes. The estimator will fail to give reasonable estimations for the lowest mode if the sampling rate is too high relative to the natural frequencies of those modes. Thus, for a system with resonant modes that are spaced more than a decade apart in frequency, the estimator cannot give reasonable results.

Of the above methods, only FFT, AIS, combined modal filter - neural networks

and combined RLS-Bairstow are able to work on-line and estimate the multi-mode natural frequency. Comparing the four methods, RLS is the simplest to compute, while the estimation accuracy of all the methods are similar. Hence, RLS is the design method chosen for the natural frequency estimator used in this research. A further analysis of the RLS method is undertaken with a view to improve the estimation accuracy for wide-band systems.

One reason why the RLS method fails to give an accurate estimation of the natural frequency for wide-band systems is that it has to deal with data that are scattered across the frequency domain [21]. Frequency domain analysis by Wahlberg and Ljung [148] reveals that the RLS method has a high-pass characteristic which becomes more pronounced as the sampling rate is increased. This high-pass characteristic gives a higher weighting to the higher frequencies and a lower weighting to the lower frequencies. Hence, the estimation for the lower frequency modes becomes inaccurate. This analysis leads designers to use pre-filtering to compensate for the low weighting at low frequencies [20, 125, 126] by giving more weighting to the lower frequencies and removing frequencies above the highest mode of interest. However, although Rovner and Franklin [126] show that prefiltering improves the estimation accuracy, particularly for the highest modes, the estimator's high-pass filter characteristic still produces inaccurate results for the lowest mode. Another reason for the estimation inaccuracies is round-off errors as a result of finite word-length in digital system realizations [9, 59]. For limited bit representations, the estimation accuracy will decrease as the sampling rate and/or the order of the estimator increase.

These reasons prompt further consideration of prefiltering design and of criteria for selecting minimal-order and appropriate sampling rates for the implementation of the RLS estimator. A new approach to obtain an accurate natural frequency estimator for flexible structure based on the prefiltering design, sam-

pling rate selection, and structure selection of an RLS estimator is proposed in this thesis.

In the following section, the on-line parameter estimation concept is briefly discussed and the implementation of an on-line estimator based on the RLS algorithm is reviewed.

4.2   On-line Parameter Estimation Using RLS

On-line plant parameter estimation is a technique for solving system identification problems by using parametric estimation methods to process sequential pairs of input-output data measurements. Fig. 4.1 [68] illustrates a schematic diagram of the on-line parameter estimation principle. An input $u(t)$ is applied to both the plant and the adjustable model. The adjustable model's parameter vector θ is then updated by the parameter adaptation algorithm. The parameter adaptation algorithm updates the adjustable model's parameters by reducing the error $\epsilon(t)$ between the plant output, $y(t)$, and the output predicted by the model, $\hat{y}(t)$, at each sampling instant t.

In general the parameter adaptation algorithm has a recursive structure as illustrated in Fig. 4.2 [70]. The new values of the estimated parameters are equal to the previous values plus a correcting term that depends on the most recent measurements. There are several approaches for deriving the parameter adaptation algorithm such as gradient descent, least-mean-squares minimization, least-squares minimization, and fuzzy logic or neural networks. While the gradient descent technique and the least-mean-squares method have a lower computational load than the least-squares method, they have a slower convergence rate [18, 47].

The first step in the estimator design is to determine a class of model. In
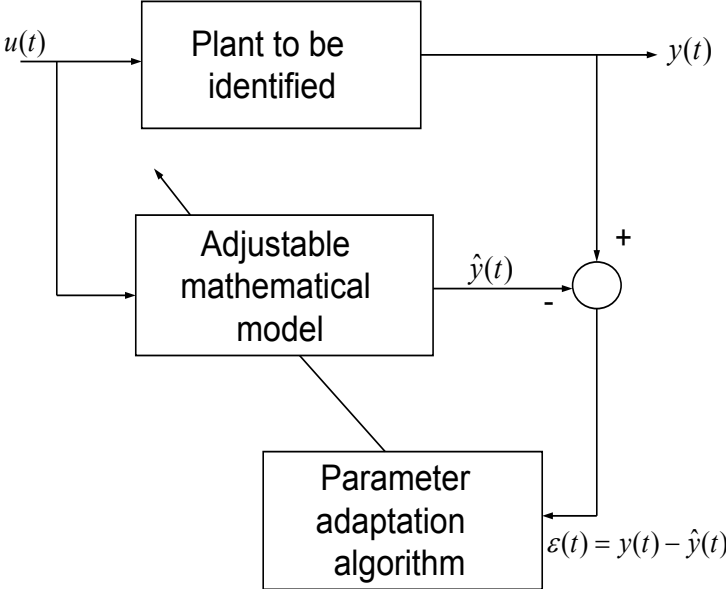
Figure 4.1. Block diagram of an on-line parameter estimator.

Figure 4.2. Recursive structure of parameter adaptation algorithm.

general a linear time-invariant discrete-time model can be given by [81]

$$y(t) = G(q, \theta)u(t) + H(q, \theta)e(t), \tag{4.1}$$

where $u(t)$ and $y(t)$ are the input and output of the system, respectively, $e(t)$ is the disturbance with zero-mean value and variance λ, and θ is the set of system parameters. The model spectrum of the disturbance is [81]

$$\Phi_e(\omega, \theta) = \lambda \left| H(e^{i\omega}, \theta) \right|^2. \tag{4.2}$$

The transfer function $G(q, \theta)$ and $H(q, \theta)$ are functions of the delay operator q^{-1}, where $q^{-k}x(t) = x(t-k)$. If the disturbance filter $H(q, \theta)$ is minimum phase, the disturbance $e(t)$ in (4.1) can be written as

$$e(t) = H^{-1}(q, \theta)y(t) - H^{-1}(q, \theta)G(q, \theta)u(t). \tag{4.3}$$

Then the optimal predictor for $y(t)$ is

$$\begin{aligned}
\hat{y}(t|\theta) &= y(t) - e(t) \\
\hat{y}(t|\theta) &= H^{-1}(q, \theta)G(q, \theta)u(t) + \left(1 - H^{-1}(q, \theta)\right)y(t). \tag{4.4}
\end{aligned}$$

Then if $H^{-1}(q, \theta)G(q, \theta)$ and $H^{-1}(q, \theta)$ are both stable, one can write:

$$H^{-1}(q, \theta)G(q, \theta) = \sum_{k=1}^{\infty} b_k q^{-k}, \tag{4.5}$$

$$H^{-1}(q, \theta) - 1 = \sum_{k=1}^{\infty} a_k q^{-k}. \tag{4.6}$$

Truncating these expansions at $k = n_b$ and $k = n_a$, respectively where n_b and n_a are the order of the polynomial $B(q)$ and $A(q)$, respectively, (4.1) can be written as

$$\left(1 + \sum_{k=1}^{n_a} a_k q^{-k}\right) y(t) = \sum_{k=1}^{n_b} b_k q^{-k} u(t) + e(t) \tag{4.7}$$

or in the compact form

$$A(q)y(t) = B(q)u(t) + e(t) \tag{4.8}$$

with

$$A(q) = 1 + a_1 q^{-1} + a_2 q^{-2} + \ldots + a_{n_a} q^{-n_a} \tag{4.9}$$

and

$$B(q) = b_1 q^{-1} + b_2 q^{-2} + \ldots + b_{n_b} q^{-n_b}. \tag{4.10}$$

It can be seen that (4.8) corresponds to (4.1) with

$$G(q, \theta) = \frac{B(q)}{A(q)}, \quad H(q, \theta) = \frac{1}{A(q)}. \tag{4.11}$$

Defining

$$\theta = [a_1, \ldots, a_{n_a}, b_1, \ldots, b_{n_b}]^T \tag{4.12}$$

and

$$\phi(t) = [-y(t-1), \ldots, -y(t-n_a), u(t-1), \ldots, u(t-n_b)]^T, \tag{4.13}$$

(4.8) can then be written as

$$y(t) = \theta^T \phi(t) + e(t). \tag{4.14}$$

Model (4.8) is known as the AutoRegressive with eXternal input (ARX) model or the least-squares model. Since the disturbance term $e(t)$ in (4.8) enters as a direct error in the equation, the model (4.8) is often referred to as an equation error model or structure [81, 135].

The limitation of the ARX model (4.8) is the lack of adequate freedom in describing the properties of the disturbance term in the governing equations of a system, resulting in a possible inaccurate estimation [20]. The estimation accuracy can be improved by describing the equation error as a moving average of white noise [20, 81]. This modifies (4.8) into

$$A(q)y(t) = B(q)u(t) + C(q)e(t) \tag{4.15}$$

with

$$C(q) = 1 + c_1 q^{-1} + c_2 q^{-2} + \ldots + c_{n_c} q^{-n_c} \tag{4.16}$$

where n_c is the order of polynomial $C(q)$. Clearly (4.15) corresponds to (4.1) with

$$G(q, \theta) = \frac{B(q)}{A(q)}, \quad H(q, \theta) = \frac{C(q)}{A(q)} \tag{4.17}$$

where now

$$\theta = [a_1, \ldots, a_{n_a}, b_1, \ldots, b_{n_b}, c_1, \ldots, c_{n_c}]^T. \tag{4.18}$$

The model given in (4.15) is referred as the AutoRegresive Moving Average with eXternal input (ARMAX) model.

Although the ARMAX model is better than the ARX model in terms of the estimation accuracy, computationally it is much more complex than the ARX model. In the computation of the coefficients θ, the ARMAX model involves non-linear optimisation [32, 47], which is complicated, computationally intensive, and also sensitive to the initial guess parameter values [32]. From this viewpoint, the ARX model offers the advantages of simpler computation and simpler implementation compared to the ARMAX model. Furthermore, since only the AR parameters (i.e., $a_1, a_2, , a_{na}$) are required to estimate the natural frequency of the system, as will be explained in Section 4.5, the ARX model is chosen as a basis for the on-line estimator.

In the computation of the unknown parameter θ in the ARX model, the RLS estimator ignores the disturbance $e(t)$, and only uses the input pair $u(t)$ and $y(t)$. Therefore, in the derivation of the RLS estimator algorithm, the disturbance $e(t)$ can be omitted from (4.14), then (4.14) can be written as

$$y(t + 1) = -\sum_{k=1}^{n_a} a_k y(t + 1 - k) + \sum_{k=1}^{n_b} b_k u(t + 1 - k) = \theta^T \phi(t) \tag{4.19}$$

where

$$\theta = [a_1, \ldots, a_{n_a}, b_1, \ldots, b_{n_b}]^T \tag{4.20}$$

and

$$\phi(t) = [-y(t), \ldots, -y(t - n_a + 1), u(t), \ldots, u(t - n_b + 1)]^T. \tag{4.21}$$

From (4.19), the adjustable prediction model can described by [70]

$$
\begin{aligned}
\hat{y}^o(t+1) &= \hat{y}\left[(t+1)|\hat{\theta}(t)\right] \\
&= -\sum_{k=1}^{n_a} \hat{a}_k(t)y(t+1-k) + \sum_{k=1}^{n_b} \hat{b}_k(t)u(t+1-k) \\
&= \hat{\theta}^T \phi(t)
\end{aligned}
\tag{4.22}
$$

where $\hat{y}^o(t+1)$ is the *a priori* predicted output and

$$
\hat{\theta}(t) = [\hat{a}_1(t), \ldots, \hat{a}_{n_a(t)}, \hat{b}_1(t), \ldots, \hat{b}_{n_b}(t)]^T.
\tag{4.23}
$$

is the estimated parameter vector at instant t. In a similar way the *a posteriori* predicted output can be given by

$$
\begin{aligned}
\hat{y}(t+1) &= \hat{y}\left[(t+1)|\hat{\theta}(t+1)\right] \\
&= -\sum_{k=1}^{n_a} \hat{a}_k(t+1)y(t+1-k) + \sum_{k=1}^{n_b} \hat{b}_k(t+1)u(t+1-k) \\
&= \hat{\theta}^T(t+1)\phi(t).
\end{aligned}
\tag{4.24}
$$

From (4.19) and (4.22) an *a priori* prediction error can be defined as

$$
\epsilon^o(t+1) = y(t+1) - \hat{y}^o(t+1).
\tag{4.25}
$$

Similarly, from (4.19) and (4.24), an *a posteriori* prediction error can be defined as

$$
\epsilon(t+1) = y(t+1) - \hat{y}(t+1).
\tag{4.26}
$$

Based on the prediction models (4.22) and (4.24), a recursive parameter adaptation algorithm with the structure

$$
\hat{\theta}(t+1) = \hat{\theta} + \Delta\hat{\theta}(t+1) = \hat{\theta}(t) + f\left[\hat{\theta}(t), \phi(t), \epsilon^o(t+1)\right]
\tag{4.27}
$$

can be formed. To design an RLS estimator, the parameter adaptation algorithm (4.27) is solved by minimizing the least-squares criterion

$$
\begin{aligned}
\hat{\theta}_N &= \arg\min_{\hat{\theta}\in\mathcal{M}} J_N(\hat{\theta}, t), \\
J_N(\hat{\theta}, t) &= \frac{1}{N}\sum_{t=1}^{N}\left[y(t) - \hat{\theta}^T(t)\phi(t-1)\right]^2,
\end{aligned}
\tag{4.28}
$$

where the arg min function is the value of $\hat{\theta}$ which minimizes the cost function $J_N(\hat{\theta}, t)$, and $\mathcal{M}$ is the domain of admissible parameters related to the ARX model. By setting the derivative of the cost function $J_N(\hat{\theta}, t)$ in (4.28) with respect to $\hat{\theta}$ equal to zero, one can obtain the RLS algorithm as [70]:

$$\hat{\theta}(t+1) = \hat{\theta} + F(t)\phi(t)\epsilon(t+1), \tag{4.29}$$

$$F(t+1)^{-1} = \lambda_1(t)F(t)^{-1} + \lambda_2(t)\phi(t)\phi^T(t), \tag{4.30}$$

$$F(t+1) = \frac{1}{\lambda_1(t)}\left[F(t) - \frac{F(t)\phi(t)\phi^T(t)F(t)}{\frac{\lambda_1(t)}{\lambda_2(t)} + \phi^T F(t)\phi(t)}\right], \tag{4.31}$$

$$\epsilon(t+1) = \frac{y(t+1) - \hat{\theta}^T(t)\phi(t)}{1 + \phi^T F(t)\phi(t)}, \tag{4.32}$$

with

$$0 < \lambda_1(t) \leq 1; \quad 0 \leq \lambda_2(t) < 2; \quad F(0) > 0 \tag{4.33}$$

where $F(t)$ is the adaptation gain matrix and $\lambda_1(t)$ and $\lambda_2(t)$ are weighting sequences.

From (4.31), it can be seen that the gain matrix $F(t)$ is varying with time, where the type of variation is determined by the choice of $\lambda_1(t)$ and $\lambda_2(t)$. The weighting sequences $\lambda_1(t)$ and $\lambda_2(t)$ have an opposite effect to the variation of $F(t)$. While $\lambda_1(t) < 1$ tends to increase $F(t)$, $\lambda_2(t) > 0$ tends to decrease it. For $\lambda_1(t) = \lambda_1 = 1$ and $\lambda_2(t) = \lambda_2 = 1$, the algorithm gives progresively less weight to the new prediction error and thus to the new measurements. Consequently, this type of variation of the adaptation gain is not suitable for the estimation of time-varying parameters. For $\lambda_1(t) = \lambda_1; 0 < \lambda_1 < 1$ and $\lambda_2(t) = \lambda_2 = 1$ the algorithm gives less weighting to the old data $(k < t)$ and maximum weight is given to the most recent error. This RLS algorithm is known as RLS with constant forgetting factor, where λ_1 is the forgetting factor. The value of the forgetting factor, λ_1, determines the response of the algorithm. A small value of λ_1 produces a fast response for tracking parameter variations, but large fluctuations

in the steady-state. On the contrary, small steady-state fluctuations with a slow tracking response are obtained for a large value of λ_1. The typical values for λ_1 which give a relatively fast but small fluctuation response are between 0.95 and 0.99 [70]. This algorithm is suited to the estimation of systems with time-varying parameters. Due to its suitability, the RLS with constant forgetting factor is used as the estimator in this research.

In the context of adaptive control, the stability of the estimator is a necessary condition for the stability of the control system. Therefore, a stable estimator must be employed in the adaptive control method.

4.3   Stability of the RLS Algorithm

The stability of an estimator is closely related to the convergence of the estimator. An estimator that converges can be said to be stable. The convergence of an estimator is determined from the behaviour of the prediction error. An estimator converges if for bounded input, $u(t)$, and bounded output, $y(t)$, the prediction error $\epsilon(t)$ is bounded. For the RLS estimator the convergence is guaranteed if the prediction error in (4.32) is bounded or

$$\lim_{t \to \infty} \epsilon(t+1) = 0. \tag{4.34}$$

The stability of the RLS algorithm can be explained by the passivity theorem. Using the passivity theorem it can be shown that for a bounded input, $u(t)$ and bounded output, $y(t)$, the prediction error $\epsilon(t)$ is bounded. To apply the passivity theorem, the equivalent feedback representation of the RLS algorithm needs to be derived.

Define the parameter error as

$$\tilde{\theta}(t) = \hat{\theta}(t) - \theta. \tag{4.35}$$

Subtracting both sides of (4.29) by θ, and taking into account (4.35), one obtains

$$\tilde{\theta}(t+1) = \tilde{\theta}(t) + F(t)\phi(t)\epsilon(t+1). \tag{4.36}$$

From the definition of the *a posteriori* prediction error $\epsilon(t+1)$ given by (4.26) and taking into account (4.19), (4.24) and (4.35), one gets

$$
\begin{aligned}
\epsilon(t+1) &= y(t+1) - \hat{y}(t+1) \\
&= \theta^T \phi(t) - \hat{\theta}^T(t+1)\phi(t) \\
&= -\tilde{\theta}^T(t+1)\phi(t) \\
&= -\phi(t)^T \tilde{\theta}(t+1). \tag{4.37}
\end{aligned}
$$

and using (4.36) one can write

$$\phi^T(t)\tilde{\theta}(t+1) = \phi^T(t)\tilde{\theta}(t) + \phi^T(t)F(t)\phi(t)\epsilon(t+1). \tag{4.38}$$

Equation (4.36), (4.37) and (4.38) define an equivalent feedback system which can be represented as in Fig. 4.3. From the figure, it can be seen that the RLS algorithm can be described as the interconnection of a linear time invariant block and a non-linear time-varying block. It is therefore reasonable to use the passivity theorem to analyse the stability of the RLS algorithm.

After the equivalent feedback representation is obtained, it can then be proven that the RLS algorithm is stable by showing that the interconnection of these two blocks is passive (see [70] for detailed proof).

In the next section, the analyses of the effect of the high-pass characteristics of the RLS, the effect of the sampling period selection, and the effect of the word-length on the estimation accuracy, are discussed. The analyses provide the justification for the use of the proposed method to improve the estimation accuracy.
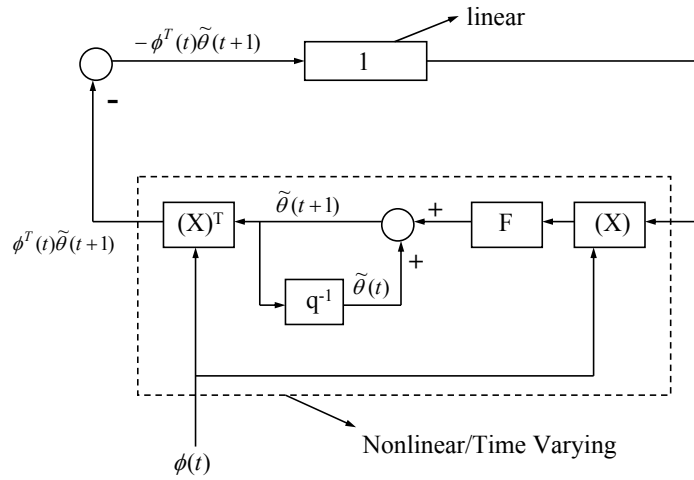
Figure 4.3. Equivalent feedback representation of RLS.

4.4 Factors Which Influence the Accuracy of RLS

As mentioned in Section 4.1 there are several factors which affect the ability of the RLS estimator to accurately estimate the natural frequencies of a flexible structure. The detailed analyses of these factors are presented in this section. The discussion is divided into three subsections. In the first subsection, the high-pass characteristic of the RLS is analysed using frequency domain analysis. In the second subsection, the effects of sampling period and finite word-length on the estimator's parameter tracking resolution are analysed. In the third subsection, an examination of the sensitivity of the poles to the parameter perturbation error is used to explain the effects of sampling period and finite word-length on the estimation accuracy.

4.4.1 RLS Characteristics

The parametric identification for a flexible structure gives biased results since the order of the estimator is much smaller than the theoretically infinite order of the plant [2, 147]. To examine the bias distribution of the RLS estimator over a range of frequencies, frequency domain analysis of the estimator is discussed in this subsection.

A recursive estimator can be considered as an algorithm that recursively minimizes a quadratic criterion in terms of the plant model prediction error or the adaptation error. The least-squares criterion in (4.28) can be written in terms of the prediction error, $\epsilon(t)$, as

$$
\begin{aligned}
\hat{\theta}_N &= \arg\min_{\hat{\theta}\in\mathcal{M}} J_N(\hat{\theta},t), \\
J_N(\hat{\theta},t) &= \frac{1}{N}\sum_{t=1}^{N}\epsilon^2(\hat{\theta},t).
\end{aligned}
\tag{4.39}
$$

For large N (i.e., N approaches infinity) the cost function $J_N(\hat{\theta},t)$ can be written as

$$
\lim_{N\to\infty} J_N(\hat{\theta},t) = J_N^*(\hat{\theta},t)
\tag{4.40}
$$

where

$$
\begin{aligned}
J_N^*(\hat{\theta},t) &= \lim_{t\to\infty}\frac{1}{N}\sum_{t=1}^{N}\epsilon^2(\hat{\theta},t) \\
&= E\{\epsilon^2(\hat{\theta},t)\},
\end{aligned}
\tag{4.41}
$$

is the asymptotic least-squares criterion. Assuming that the RLS estimator converges, the estimated parameter $\hat{\theta}_N$ will converge to the optimal parameter estimation $\hat{\theta}^*$, and can be written as [148]

$$
\hat{\theta}_N \to \hat{\theta}^*, \quad as \quad N \to \infty
\tag{4.42}
$$

where

$$
\hat{\theta}^* = \arg\min_{\hat{\theta}\in\mathcal{M}} J_N^*(\hat{\theta},t),
\tag{4.43}
$$

Applying the Parseval Theorem to (4.41), a frequency interpretation of the asymptotic least-squares criterion can be obtained as [148]

$$\hat{\theta}^* = \arg\min_{\hat{\theta}\in\mathcal{M}} \int_{-\pi/T}^{\pi/T} \Phi_\epsilon(e^{j\omega})d\omega, \tag{4.44}$$

where $\Phi_\epsilon(e^{j\omega})$ is the spectrum of the prediction error and T is the sampling period. Equation (4.44) shows how the cost function of the RLS criterion in terms of the adaptation error, $\epsilon(t)$, is distributed in frequency. By expressing the prediction error in terms of the bias between the model and the estimation model, (4.44) can be used to assess how the bias is distributed in frequency. To express the prediction error, $\epsilon(t)$, in the estimation model's parameters $\hat{\theta}$, write $\epsilon(t)$ as the difference between the model output, $y(t)$, and the estimation output, $\hat{y}(t)$,

$$\epsilon(t) = y(t) - \hat{y}(t). \tag{4.45}$$

The model output, $y(t)$, is given in (4.1) and the optimal estimation output, $\hat{y}(t)$, is given by

$$\hat{y}(t) = \hat{H}^{-1}(q,\hat{\theta})\hat{G}(q,\hat{\theta})u(t) + \left(1 - \hat{H}^{-1}(q,\hat{\theta})\right)y(t), \tag{4.46}$$

which is obtained by replacing the parameters $H(q,\theta)$ and $G(q,\theta)$ in (4.4) with the estimation parameters $\hat{H}(q,\hat{\theta})$ and $\hat{G}(q,\hat{\theta})$. Using (4.1) and (4.46), the prediction error (4.45) can be written as

$$
\begin{aligned}
\epsilon(t) &= y(t) - \hat{y}(t) \\
&= G(q)u(t) + H(q)e(t) - \hat{H}^{-1}(q)\hat{G}(q)u(t) - \left(1 - \hat{H}^{-1}(q)\right)y(t) \\
&= \hat{H}^{-1}(q)\left[G(q) - \hat{G}(q)\right]u(t) + \hat{H}^{-1}(q)H(q)e(t) \\
&= \hat{H}^{-1}(q)\left\{\left[G(q) - \hat{G}(q)\right]u(t) + \left[H(q) - \hat{H}(q)\right]e(t)\right\} + e(t).
\end{aligned}
\tag{4.47}
$$

To obtain the spectrum of (4.47), write

$$
\begin{aligned}
E\{\epsilon^2(t,\hat{\theta})\} &= |\hat{H}^{-1}(q)|^2\left[|G(q) - \hat{G}(q)|^2 E\{u^2(t)\} + |H(q) - \hat{H}(q)|^2 E\{e^2(t)\}\right] \\
&\quad + E\{e^2(t)\}.
\end{aligned}
\tag{4.48}
$$

Taking the Fourier transform of (4.48) and neglecting the terms that do not depend upon the estimated parameters, one obtains

$$\Phi_\epsilon(e^{j\omega}) = |\hat{H}^{-1}(e^{j\omega})|^2 \left[|G(e^{j\omega}) - \hat{G}(e^{j\omega})|^2 \Phi_u(\omega) + |H(e^{j\omega}) - \hat{H}(e^{j\omega})|^2 \Phi_e(\omega)\right],$$

(4.49)

where $\Phi_u(\omega)$ and $\Phi_e(\omega)$ are the spectrums of input and disturbance, respectively. Inserting the spectrum of the prediction error (4.49) into (4.44), one obtains

$$\begin{aligned}
\hat{\theta}^* &= \arg\min_{\hat{\theta}\in\mathcal{M}} \int_{-\pi/T}^{\pi/T} |\hat{H}^{-1}(e^{j\omega})|^2 \\
&\quad \times \left[|G(e^{j\omega}) - \hat{G}(e^{j\omega})|^2 \Phi_u(\omega) + |H(e^{j\omega}) - \hat{H}(e^{j\omega})|^2 \Phi_e(\omega)\right] d\omega.
\end{aligned}$$

(4.50)

Equation (4.50) is an interpretation of the asymptotic least-squares criterion as a function of the system model in the frequency domain. It can be seen that the optimum estimation value $\hat{\theta}^*$ is influenced by the weighted error between the true system parameter G and the estimated system parameter $\hat{G}$. Optimum $\hat{\theta}^*$ is obtained by minimizing the bias between $\hat{G}$ and G. The weighting function, $|\hat{H}^{-1}(e^{j\omega})|^2$, determines how much weight the estimator will give to minimize the bias contribution at each particular frequency. For a large weight in a particular frequency range, the algorithm will tend to give small bias, resulting in an accurate estimation in that range [88].

For RLS using the ARX model the weighting function $|\hat{H}^{-1}(e^{j\omega})|^2$ is equal to $|\hat{A}(e^{j\omega})|^2$ (see (4.11)). For any order and any random coefficients $|\hat{A}(e^{j\omega})|^2$ has a high-pass filter (HPF) profile as illustrated in Fig. 4.4. Therefore, for a broadband input $\phi_u(\omega)$, the RLS algorithm will give a higher weighting to higher frequency components and a lower weighting to the lower frequency components. This will result in higher accuracies for the estimation of higher modes and, conversely, lower accuracies for the estimation of lower modes. As T decreases, the passband of $|\hat{A}(e^{j\omega})|^2$ will shift to the right, resulting in a corresponding reduction

of $|\hat{H}^{-1}(e^{j\omega})|^2$ for the same frequency. Consequently, for smaller T, the RLS will produce even poorer estimates of the lower modes.
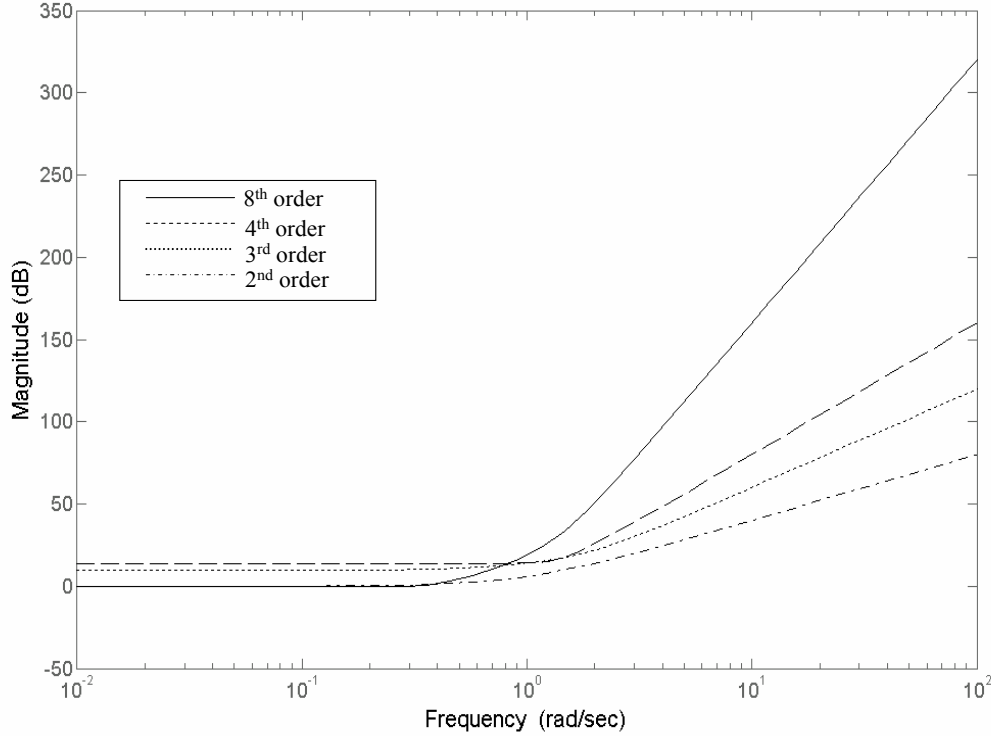

Figure 4.4. Frequency responses of $\hat{A}(e^{j\omega})$ for different order.

Prefiltering can be used to compensate for the low weighting in the low frequency ranges, thereby improving the accuracy of estimation in the low frequency ranges. Let $L(q)$ be a prefilter that is applied to both $u(t)$ and $y(t)$. Then from (4.47), the filtered prediction error can be written as

$$
\begin{aligned}
\epsilon(t) &= L(q)\left[y(t) - \hat{y}(t)\right] \\
&= L(q)\left[G(q)u(t) + H(q)e(t) - \hat{H}^{-1}(q)\hat{G}(q)u(t) - \left(1 - \hat{H}^{-1}(q)\right)y(t)\right] \\
&= L(q)\left[\hat{H}^{-1}(q)\left[G(q) - \hat{G}(q)\right]u(t) + \hat{H}^{-1}(q)H(q)e(t)\right] \\
&= L(q)\hat{H}^{-1}(q)\left\{\left[G(q) - \hat{G}(q)\right]u(t) + \left[H(q) - \hat{H}(q)\right]e(t)\right\} + L(q)e(t).
\end{aligned}
$$

$$(4.51)$$

The optimal value of the estimated parameter in (4.50) can be written as

$$
\begin{aligned}
\hat{\theta}^* &= \arg\min_{\theta \in \mathcal{M}} \int_{-\pi/T}^{\pi/T} |L(e^{j\omega})|^2 |\hat{H}^{-1}(e^{j\omega})|^2 \\
&\quad \times \left[|G(e^{j\omega}) - \hat{G}(e^{j\omega})|^2 \phi_u(\omega) + |H(e^{j\omega}) - \hat{H}(e^{j\omega})|^2 \phi_e(\omega) \right] d\omega.
\end{aligned}
$$

$$(4.52)$$

From (4.52) it can be seen that prefiltering modifies the weighting function from $|\hat{H}^{-1}(e^{j\omega})|^2$ to $|L(e^{j\omega})|^2 |\hat{H}^{-1}(e^{j\omega})|^2$, thus increase the flexibility to set the weighting function. Therefore, the overall weighting at the low frequencies can be increased by choosing a prefilter $L(q)$ with a high gain at low frequencies.

From the frequency domain analysis in this subsection, it can be seen that the RLS method has a tendency to emphasize the weightings attached to high frequencies. This characteristic becomes more pronounced as T decreases, and this implies that, without prefiltering and for very small T, the RLS method will give inaccurate results for low frequency estimations. The effect of sampling period and finite word-length on the estimation accuracy from the parameter tracking resolution viewpoint is investigated further in the next subsection.

4.4.2 Parameter Tracking Resolution

The role of the estimator in an adaptive control system is to identify and track changes in the plant parameters, no matter how small the changes are, and to produce accurate estimates which reflect these changes. This requirement is directly influenced by the selection of the sampling period for the estimator as discussed below.

The influence of the sampling period T on the estimation tracking resolution can be illustrated by mapping the plant poles from the s-plane to the z-plane for different values of T. Assume that, for a fixed-value of T, as the plant changes from one model to another, one of the plant poles changes accordingly in the

s-plane from $s_1 = \sigma_1 + j\omega_1$ to $s_2 = \sigma_2 + j\omega_2$. The corresponding pole locations in the z-plane are

$$
\begin{aligned}
z_1 &= e^{s_1 T} = e^{\sigma_1 T} e^{j\omega_1 T} = |e^{\sigma_1 T}|\angle\omega_1 T, \\
z_2 &= e^{s_2 T} = e^{\sigma_2 T} e^{j\omega_2 T} = |e^{\sigma_2 T}|\angle\omega_2 T.
\end{aligned}
\tag{4.53}
$$

The difference between the arguments of z_1 and z_2 is

$$
\Delta\Phi = |(\omega_1 - \omega_2)T| = 2\pi T|f_1 - f_2|.
\tag{4.54}
$$

If, however, T changes from T_1 to T_2, where $T_2 = nT_1(n > 0)$, then the ratio of the corresponding differences between the arguments of z_1 and z_2 can be written as

$$
\frac{\Delta\Phi_1}{\Delta\Phi_2} = \frac{T_1|f_1 - f_2|}{T_2|f_1 - f_2|} = \frac{T_1}{nT_1} = \frac{1}{n}.
\tag{4.55}
$$

From (4.55) it can be seen that, as T becomes n-times larger, the differences between the arguments of z_1 and z_2 also becomes n-times larger, thus resulting in more accurate estimates. The following example illustrates this effect.

Consider a plant that changes from Model A with natural frequency 9.77 Hz to Model B with natural frequency 7.53 Hz. The transfer functions of Model A, M_a, and Model B, M_b, are as follows:

$$
M_a = \frac{0.02768}{s^2 + 1.229s + 3775}, \quad M_b = \frac{0.3398}{s^2 + 0.9461s + 2238}.
$$

The models are both sampled with different sampling periods, $T_1 = 1/500$ second and $T_2 = 1/50$ second (i.e., $n = 10$). The locations of the plant poles in the z-plane for differing T are shown in Fig. 4.5. From the figure it can be seen that, when the plant changes from M_a to M_b, $\Delta\Phi_2 = 16.2^o$ associated with T_2 is 10-times larger than $\Delta\Phi_1 = 1.62^o$ associated with T_1. This demonstrates that the estimator's capacity to resolve small changes in natural frequency between one

model and another can be compromised by the use of inappropriately selected high sampling rates when the bit-precision of the computing platform is limited. The higher the sampling rate, the smaller the argument and, consequently, the higher the bit-precision required.
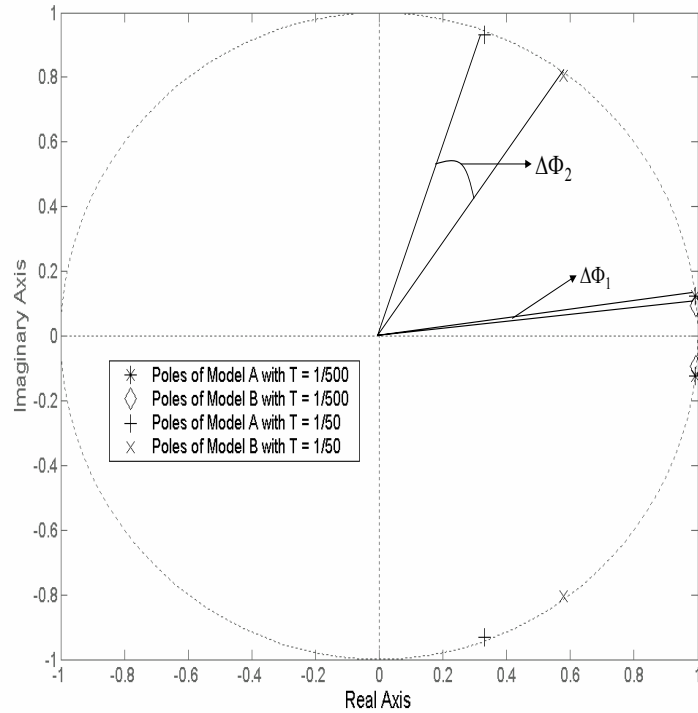

Figure 4.5. Effect of sampling period on pole location.

The determination of the sampling period of the estimator is dependent on the natural frequency of interest in the estimated system. If the sampling rate is too high relative to the natural frequency, the resolution of the estimator will be low and hence the estimation results will be inaccurate. Empirical results show that a sampling rate between 4 to 20 times the natural frequency of the system gives accurate estimates. This sampling rate range is in agreement with recommendations from the literature [33, 45, 70, 107, 123, 150].

4.4.3 Parameter Perturbation Error

The RLS estimator (4.29) to (4.32) is realized as an Infinite Impulse Response (IIR) filter. In a digital hardware realization, the filter's coefficients are quantized and stored as finite-word length values in a register. Due to the limitation of the word-length, quantization errors occur which perturb the parameters of the estimator and hence affect the estimator accuracy. This in turn is effected by the sampling rate and the order of the estimator, as shown in the following analysis.

The IIR filter has the following transfer function [117]

$$G(z) = \frac{\sum_{k=0}^{n_b} b_k z^{-k}}{1 + \sum_{k=1}^{n_a} a_k z^{-k}}. \tag{4.56}$$

When the IIR filter is realized with quantized coefficients, its tranfer function is modified as follows

$$G_q(z) = \frac{\sum_{k=0}^{n_b} b_{qk} z^{-k}}{1 + \sum_{k=1}^{n_a} a_{qk} z^{-k}} \tag{4.57}$$

where the quantized coefficients $\{b_{qk}\}$ and $\{a_{qk}\}$ are obtained from their unquantized counterparts $\{b_k\}$ and $\{a_k\}$

$$
\begin{aligned}
a_{qk} &= a_k + \Delta a_k & k = 1, 2, \ldots, n_a \\
b_{qk} &= b_k + \Delta b_k & k = 0, 1, 2, \ldots, n_b
\end{aligned}
\tag{4.58}
$$

and where $\{\Delta a_k\}$ and $\{\Delta b_k\}$ are the quantization errors. The denominator of $G(z)$ in (4.56) can be expressed as

$$A(z) = 1 + \sum_{k=1}^{n_a} a_k z^{-k} = \prod_{k=1}^{n_a} (1 - p_k z^{-k}) \tag{4.59}$$

where $\{p_k\}$ are the poles of $A(z)$. Similarly, the denominator of $G_q(z)$ in (4.57) can be expressed as

$$A_q(z) = 1 + \sum_{k=1}^{n_a} a_q z^{-k} = \prod_{k=1}^{n_a} (1 - p_{qk} z^{-k}) \tag{4.60}$$

where

$$p_{qk} = p_k + \Delta p_k, \qquad k = 1, 2, \ldots, n_a \qquad (4.61)$$

and Δp_k is the error or perturbation resulting from the quantization of the filter coefficients. The relationship between the total perturbation error for the ith pole, Δp_i, and the quantization error $\{\Delta a_k\}$ can be given by [117]

$$
\begin{aligned}
\Delta p_i &= \sum_{k=1}^{n_a} \frac{\partial p_i}{\partial a_k} \Delta a_k \\
&= -\sum_{k=1}^{n_a} \frac{p_i^{n_a-k}}{\prod_{l=1, l \neq i}^{n_a} (p_i - p_l)} \Delta a_k.
\end{aligned}
\qquad (4.62)
$$

Effectively, the expression for Δp_i in (4.62) gives a measure of the sensitivity of the ith pole to changes in the coefficients $\{a_k\}$ due to the quantization error for Δa_k. From (4.62) it can be seen that the perturbation error also depends on:

1. the order of the estimator n_a. The higher the order n_a, the larger the error for a fixed word-length;

2. the sampling rate, which determines the separation of the poles. As the sampling rate increases, the poles are drawn closer together, i.e., the term $(p_i - p_l)$ representing the distance between poles $\{p_l\}$ to p_i (where $l \neq i$) becomes smaller. This results in a larger perturbation error Δp_i. This effect is illustrated in Fig. 4.5, where the separation of the poles for a given model is decreased when the sampling rate is increased.

4.5 Design of the Natural Frequency Estimator for Flexible Structures

The analysis in Section 4.4 shows that there are several factors which influence the accuracy of an RLS estimator. The factors can be summarized as the:

1. High-pass characteristic of the RLS algorithm. The RLS algorithm gives higher gain for signals at higher frequencies, and consequently produces less accurate results for lower frequencies.

2. Selection of the sampling period T. If the sampling period is too short with respect to the mode of interest, it will make the estimation inaccurate for that particular mode.

3. Parameter word-length representation. Higher estimation accuracy will be obtained as the word-length for the IIR filter implementation is increased.

4. Order of the estimator. The higher the order of the estimator, the larger the quantization error, thus resulting in less accurate estimation.

The high-pass characteristics of the RLS algorithm can be compensated for by adding a prefilter to the estimator. The prefilter increases the weighting at the frequency ranges of concern. However, as shown in [126] prefiltering alone is not adequate for obtaining accurate estimations for the lower modes of wide-band systems due to the miss match between the chosen sampling rate and the frequencies of the lower modes. Using longer word lengths to improve the accuracy is not always possible due to implementation cost and availability constraints. Therefore a combination of prefiltering design, sampling period selection and estimator order selection is required if improvements in estimation accuracy are to be achieved.

What follow is an exposition of a design methodology for a multi-mode natural frequency estimator with superior performance in terms of accuracy and simplicity to known natural frequency estimators described in the literature.

Rule of the estimator

In the proposed design, a bank of band-pass filters (BPFs) is used in the prefiltering process to decompose a system into several bands in the frequency domain.

Each band can be described as a second-order system which represents a system mode of interest. A second-order estimator with an appropriate sampling period for a specific mode is then used to estimate the natural frequency for that mode. To estimate the multi-mode natural frequency, a parallel combination of prefiltered second-order estimators can be employed.

Estimator Design

A linear time-invariant system can be band-wise approximated by the summation of lower order systems [142]. Given a plant with a transfer function $G(q)$, consider the second-order approximation $G_m(q) = G(q)L_m(q)$ where $L_m(q)$ is a BPF with centre frequency ω_m

$$G_m(q) = \frac{b_{1m}q^{-1} + b_{2m}q^{-2}}{1 + a_{1m}q^{-1} + a_{2m}q^{-2}}. \tag{4.63}$$

Then the transfer function of the system can be described as

$$G(q) = \sum_{m=1}^{M} G_m(q) \tag{4.64}$$

where M is the maximum number of modes of interest. From (4.64), it can be seen that the plant can be approximated as a sum of M decoupled systems $G_m(q)$. The identification of plant $G(q)$ can therefore be achieved by using cascaded banks of M-parallel band-pass prefilters $L_m(q)$ and M-parallel second-order RLS estimators operated in a chain fashion, with each chain targeting an individual mode. Assuming that the structure natural frequencies are widely spaced and independent of each other (which is valid for many flexible beam structures [90]), each mode can be identified independently through their respective chains. The cut-off of the band-pass prefilter within each chain is chosen to admit the full range of frequencies associated with its respective mode for all possible loading conditions.

The RLS-based estimator within the chain uses a specific sampling rate appropriate for that chain's mode of interest, thus allowing the RLS pass-band to

be positioned over the mode of interest. The sampling rate is chosen to be greater than 4 times the upper-bound frequency and less than 20 times the lower-bound frequency of that mode, thus satisfying the consideration discussed in Section 4.4. The upper and lower bound frequencies of each mode for different loadings can be predetermined through modal testing of the structure. In this way, the proposed multi-mode estimator bank can effectively and accurately identify the multiple resonant modes over a wide bandwidth for different loading conditions. Different sampling rates can be applied to the various mode estimators without affecting the stability of the overall estimator, because the estimator for each mode is independent of the estimators for all the other modes.

To derive the natural frequency estimation algorithm for the mth mode using RLS, rewrite (4.63) as

$$G_m(z) = \frac{b_{1m}z + b_{2m}}{z^2 + a_{1m}z + a_{2m}}.$$ (4.65)

Applying the bilinear transformation

$$z = \frac{2f_s + s}{2f_s - s}$$ (4.66)

to (4.65), where f_s is the specific sampling rate for the mth mode, gives

$$G_m(s) = \frac{c_0 s^2 + c_1 s + c_2}{s^2 + d_1 s + d_2}$$ (4.67)

where

$$
\begin{aligned}
c_0 &= \frac{b_{1m} + b_{2m}}{1 - a_{1m} + a_{2m}}, \\
c_1 &= \frac{4f_s b_{2m}}{1 - a_{1m} + a_{2m}}, \\
c_2 &= \frac{4f_s^2(b_{1m} + b_{2m})}{1 - a_{1m} + a_{2m}}, \\
d_1 &= \frac{4f_s - 4f_s a_{2m}}{1 - a_{1m} + a_{2m}}, \\
d_2 &= \frac{4f_s^2(1 + a_{1m} + a_{2m})}{1 - a_{1m} + a_{2m}}.
\end{aligned}
$$

Comparing the denominator of (4.67) with the denominator of (2.47), the natural frequency associated with the mth mode can be identified as

$$\omega_m = 2f_s \sqrt{\frac{1 + a_{1m} + a_{2m}}{1 - a_{1m} + a_{2m}}}.$$ (4.68)

From (4.68), it can be seen that ω_m depends only on the coefficients of the denominator of (4.65) which decide the poles of that mode. As shown in Section 2.5 in Chapter 2, the locations of the system's poles are not influenced by mode truncation. Hence, truncation of the higher modes in the modeling will only give inaccurate locations for the system's zeros, but not for the system's poles. The natural frequency estimation obtained from (4.68) is therefore not affected by mode-truncation. This implies that the proposed natural frequency estimator is robust to unmodeled dynamics caused by mode truncation.

Estimator Algorithm

The algorithm for each component estimator is therefore specified as follows:

1. Find the parameters of (4.63) using the RLS algorithm

$$\hat{\theta}(t + 1) = \hat{\theta} + F(t)\phi(t)\epsilon(t + 1),$$ (4.69)

$$F(t + 1)^{-1} = \lambda_1(t)F(t)^{-1} + \lambda_2(t)\phi(t)\phi^T(t),$$ (4.70)

$$F(t + 1) = \frac{1}{\lambda_1(t)}\left[F(t) - \frac{F(t)\phi(t)\phi^T(t)F(t)}{\frac{\lambda_1(t)}{\lambda_2(t)} + \phi^T F(t)\phi(t)}\right],$$ (4.71)

$$\epsilon(t + 1) = \frac{y(t + 1) - \hat{\theta}^T(t)\phi(t)}{1 + \phi^T F(t)\phi(t)}.$$ (4.72)

2. Calculate the corresponding natural frequency using (4.68).

Hence, the M-modes of interest can be collectively identified by a bank of M parallel estimators.

For a single-input single-output system the number of multiply-accumulate operations for the RLS algorithm is of the order of $4(2M)^2$, where $2M$ is the

order of the system [61]. Therefore, in addition to increasing the estimation accuracy, the proposed M-parallel second-order estimator bank also reduces the number of mathematical operations from $4(2M)^2$ to around $16M$ operations. For example, for M=3, there is a reduction in the number of operations from 144 operations to 48 operations (i.e., a 66.7% reduction). The reduction becomes more significant for larger M (e.g., 90% for $M = 10$).

The effectiveness of the proposed estimator is evaluated through simulation and experimental studies which are discussed in the following sections. A real-time estimator for estimating the natural frequency estimator of the first three modes of the beam is implemented using the Simulink Real-Time Workshop C S-function.

4.6 Simulation Studies of the Proposed Natural Frequency Estimator

In this section, two sets of simulation studies are undertaken to evaluate the effectiveness of the proposed method.

The results of the first set of simulations demonstrate how the choice of pre-filtering and sampling period affect the accuracy of the estimator. They further show that (i) the decomposition of a plant into several bands according to its modes using a bank of BPFs improves the accuracy of estimation, and (ii) further improvement can be achieved by using an appropriate sampling period for each specific band.

In the second set of simulations, the estimator is used to estimate the natural frequencies of the cantilever beam models. In this set of simulations, the accuracy and convergence rate of the proposed estimator in tracking the changes to the natural frequencies of the system are evaluated.

4.6.1   Effects of Prefiltering and T Selection

For the first set of simulations, the twentieth-order Model 4 (the unloaded model) obtained from Chapter 2 is considered to be a true model. Model 4 is chosen in this simulation because this model has the highest first mode natural frequency. Therefore if inaccurate estimations of lower mode frequencies are obtained for this model, inaccurate estimations would also be obtained for the lower modes in the other models (Model 1 to Model 3). From the ten modes of the model, only the first three modes are estimated.

Four simulation cases for the beam model are designed as follows: the first case uses no prefiltering; the second case uses a single sixth-order estimator with low-pass filter (LPF); the third case uses three parallel second-order estimators, each with a BPF and a common value of T; the fourth case uses three parallel second-order estimators, each with a BPF and a specifically selected T according to the mode of concern. To minimize frequencies outside the modes of concern from entering the estimator, the cut-off frequency for the LPF is set slightly higher than the natural frequency of the third mode. Similarly, the upper cut-off frequencies of the three BPFs: f_{u1}, f_{u2}, and f_{u3}, are set slightly higher than the first, second, and third natural frequencies, respectively. To isolate each mode separately, the lower cut-off frequencies of the three BPFs: f_{l1}, f_{l2}, and f_{l3}, are set in such a way that the side lobes of each filter do not overlap. In the first three simulation cases, the sampling periods are all equal to $T = 0.001$ sec. In the last simulation case, the sampling periods are $T_1 = 0.02$ sec, $T_2 = 0.002$ sec, and $T_3 = 0.001$ sec. The FRF of the estimation results for the four simulation cases are shown in Figs. 4.6 to 4.9.

From Figs. 4.6 to 4.9, it can be seen that the choice of prefilter $L(q)$ and sampling period T influence the estimation accuracy. Fig. 4.6 shows that without prefiltering the estimator produces a poor result. Fig. 4.7 shows that using a

single LPF with a value of T, which is based on the third mode frequency, gives an accurate estimation for the third mode, a less accurate estimation for the second mode, and a false estimation for the first mode. This demonstrates that the LPF alone cannot compensate for the HPF characteristic of the RLS algorithm, and that the RLS cannot handle a high-order system where the natural frequencies are separated by more than one decade. This problem can be improved, as shown in Fig. 4.8, by using a parallel set of second-order estimators with a bank of BPFs where both third and second modes are correctly estimated. However, the first mode estimation is still inaccurate. This is because the 1 kHz sampling rate used is far higher than the first-mode frequency. Further improvement in the estimation accuracy for all modes can be obtained by using the proposed multi-rate, multi-mode estimator in which independent sampling rates are assigned to the three parallel second-order estimators, as confirmed by Fig. 4.9.
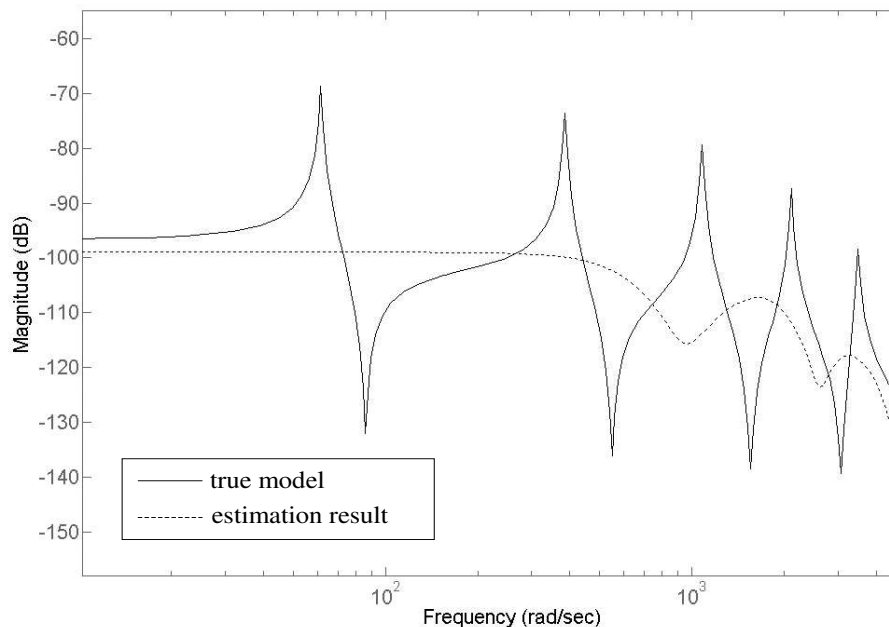
Figure 4.6. Estimation result without prefiltering.
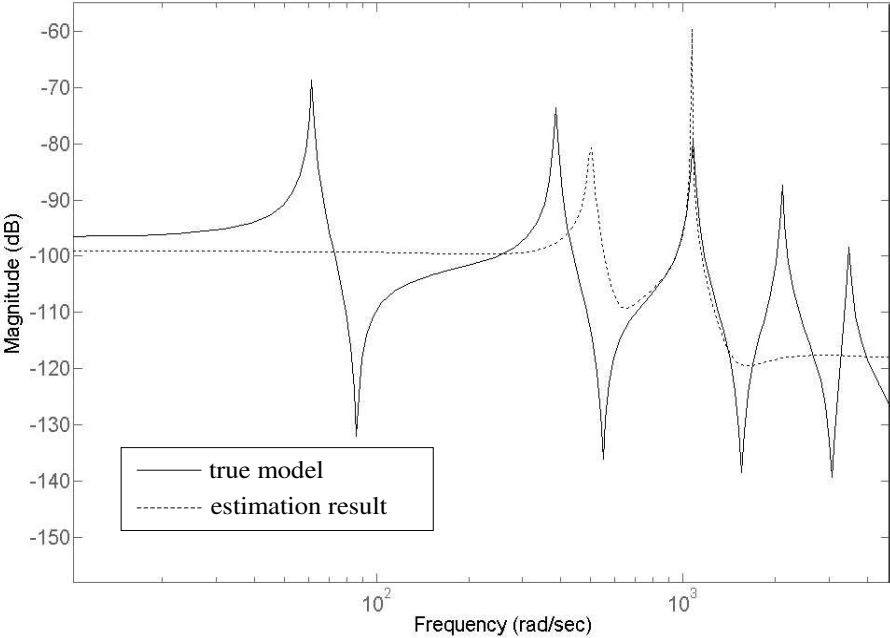
Figure 4.7. Estimation result with prefiltering using single LPF.
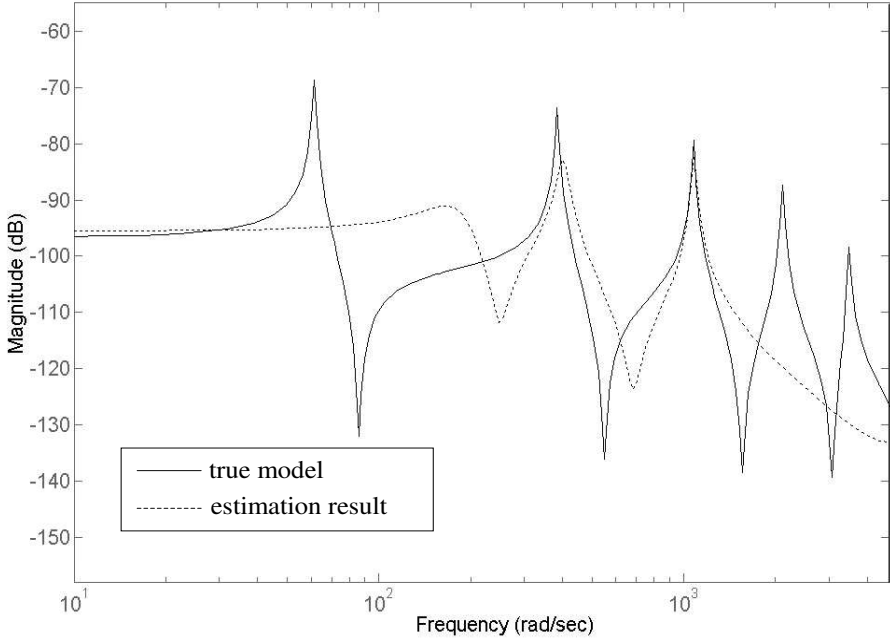
Figure 4.8. Estimation result with prefiltering using BPFs.
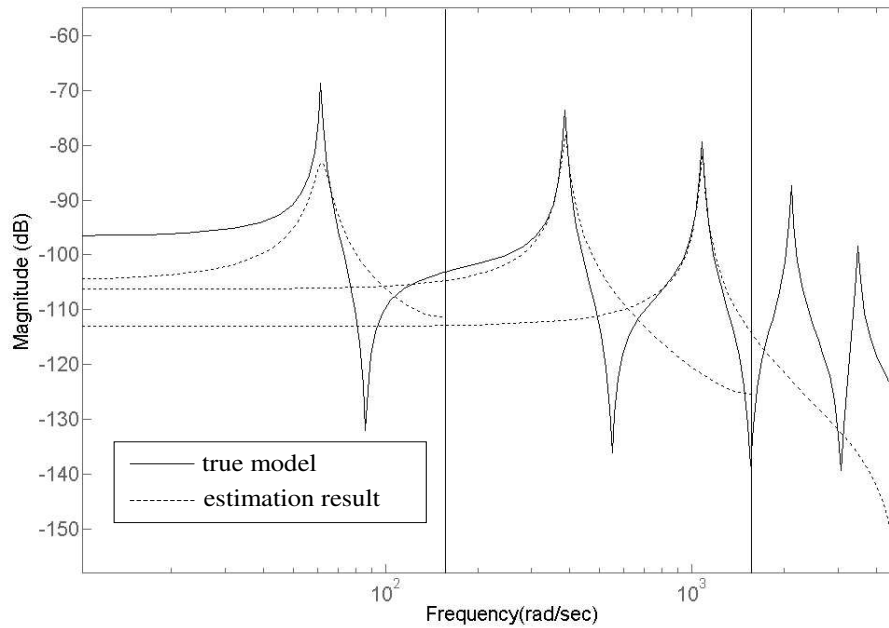
Figure 4.9: Estimation result with prefiltering using BPFs and different sampling periods.

4.6.2 Natural Frequency Estimator for Cantilever Beam Models

In the second set of simulations, a bank of three parallel second-order estimators, E_1 to E_3, is implemented. The same forgetting factor $\lambda_1 = 0.98$ is chosen for all the estimators. This value is chosen as a trade-off between fast response to track parameter variations and fluctuations in the steady-state as mentioned in Section 4.2. The estimators are used to estimate the first three natural frequencies of the simulation models, Model 1 to Model 4, with natural frequencies as shown in Table 2.5. To have appropriate sampling periods for each mode in the models, as discussed in Section 4.4, the sampling periods for E_1, (T_1), E_2, (T_2), and E_3, (T_3), are chosen as 0.02 sec, 0.002 sec and 0.001 sec, respectively. The sampling rate selected for the simulation is 1 kHz, therefore the sampling periods T_1 and T_2 are obtained by down-sampling the simulation rate by 20 and 2, respectively.

Considering the natural frequencies of the models, the upper and lower cut-off frequencies for band-pass filters L_1, L_2 and L_3 are chosen as follows: $f_{u1} = 20$ Hz, $f_{l1} = 2$ Hz, $f_{u2} = 90$ Hz, $f_{l2} = 30$ Hz, $f_{u3} = 200$ Hz, $f_{l3} = 100$ Hz. The filter order chosen is based on a trade-off between attenuation and latency. Higher order filters give better attenuation but they increase the delay and take longer to compute. Experiments show that a sixth-order BPF gives adequate attenuation for signals outside the ranges of interest, then all the filters are implemented as sixth-order Butterworth digital filters. The schematic diagram of the natural frequency estimator bank is shown in Fig. 4.10. Four simulation cases referred to as Est.1 to Est.4 cases are considered. The Est.1 and Est.2 cases assess the accuracy of the estimator bank, and the Est.3 and Est.4 cases investigate how the estimator copes with dynamic loading conditions. A white noise disturbance is used in all cases.
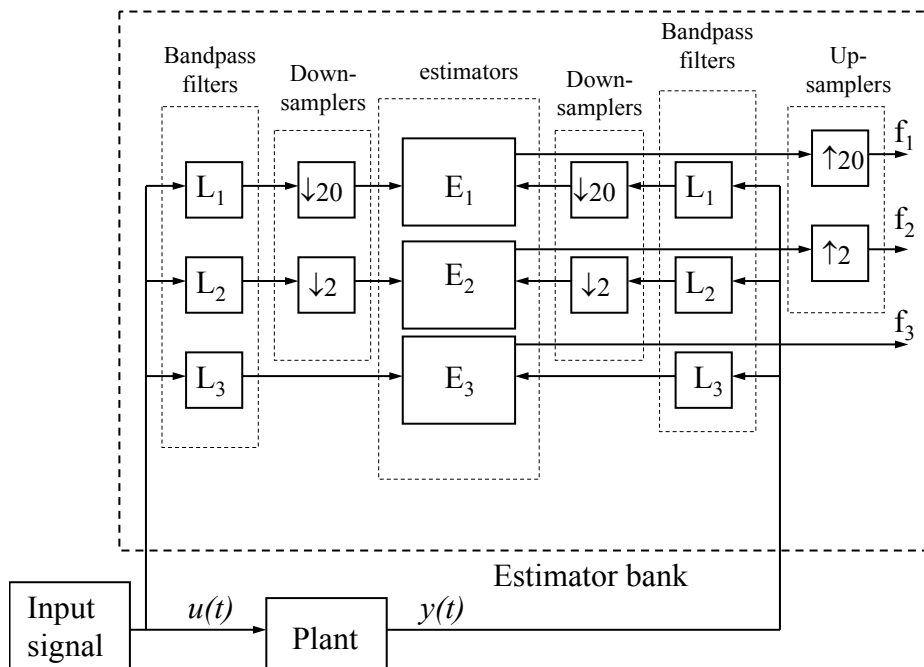
Figure 4.10. Schematic diagram for natural frequency estimator.

Est.1 and Est.2 cases

In the Est.1 and Est.2 cases, Model 1 and Model 4, respectively, are used. These cases represent the two extreme loading models for the beam. The estimates for Model 1 are shown in Fig. 4.11, and the magnified portion of the steady-state condition, which illustrates the accuracy of the estimates, is shown in Fig. 4.12. Similarly the estimates for Model 4 are shown in Fig. 4.13, and the corresponding magnified capture is shown in Fig. 4.14. From Figs. 4.11 to 4.14, it can be seen that the estimator converges to the true values of the models and gives very accurate results for all modes (the first three modes) of the models with bias errors ranging from 0.06% for the first mode of Model 4 to 0.2% for the first mode of Model 1. The results show that the largest bias error occurred for the first mode of Model 1, which has the lowest natural frequency of all the models.

Est.3 and Est.4 cases

In the Est.3 and Est.4 cases, two loading configuration sequences namely $1 \rightarrow 3 \rightarrow 4$, and $1 \rightarrow 2 \rightarrow 4$, respectively, are tested. The result for the Est.3 and Est.4 cases are shown in Figs. 4.15 and 4.16, respectively. Figs. 4.15 and 4.16 show that the estimator is able to track the varying parameters of the models when the loading is suddenly changed. The convergence time of the estimator depends on the magnitude of the loading change between the initial condition and the final condition. The larger the magnitude the longer the convergence time. The two figures also reveal that regarding the use of different sampling periods for each mode, the convergence rate of the mode estimators is slower for the lower mode than for the higher mode. From the figures, it can be seen that the convergence time ranges from around 1 second (for the third mode when the model changes from Model 1 to Model 2) to about 7 seconds (for the first mode when the model changes from Model 3 to Model 4), which is fast enough to be used in a practical adaptive control system.
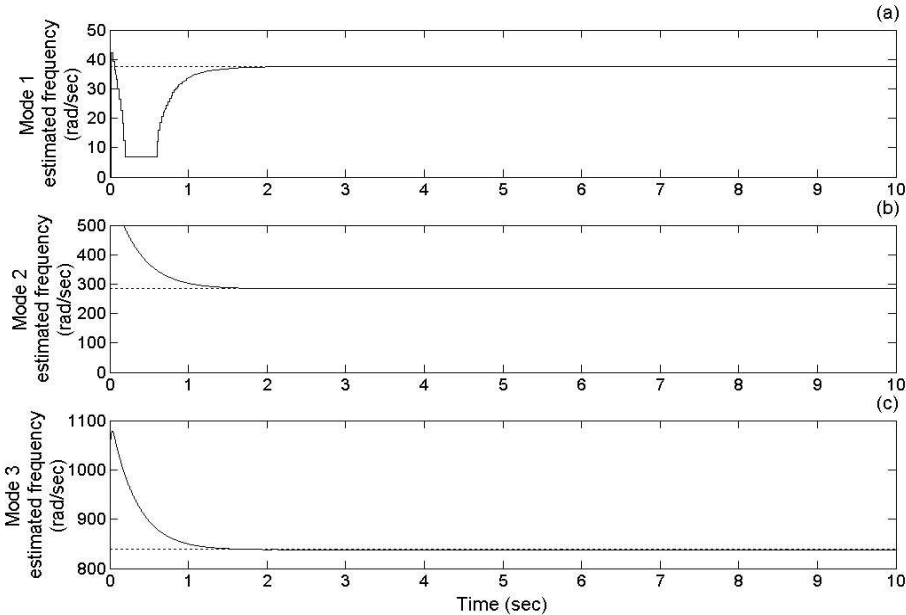
Figure 4.11. Estimation results for Model 1.
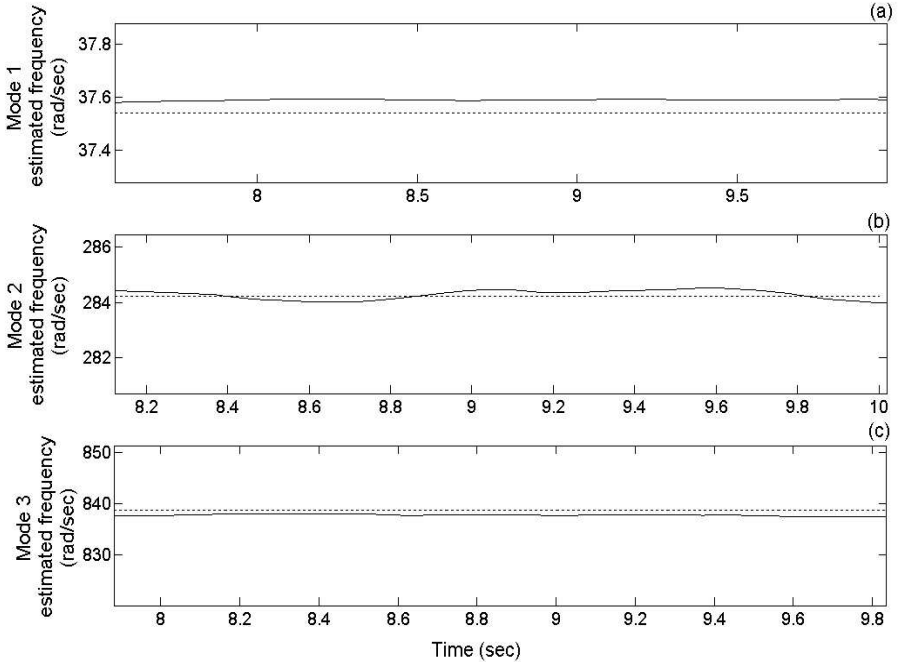
Figure 4.12. Magnified steady-state results for Model 1 estimation.
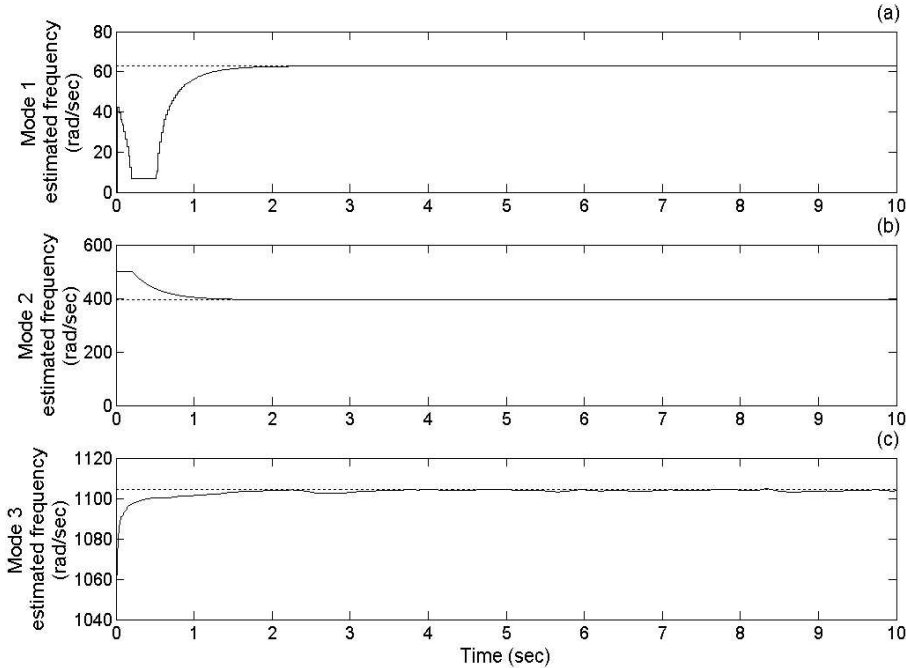
Figure 4.13. Estimation results for Model 4.
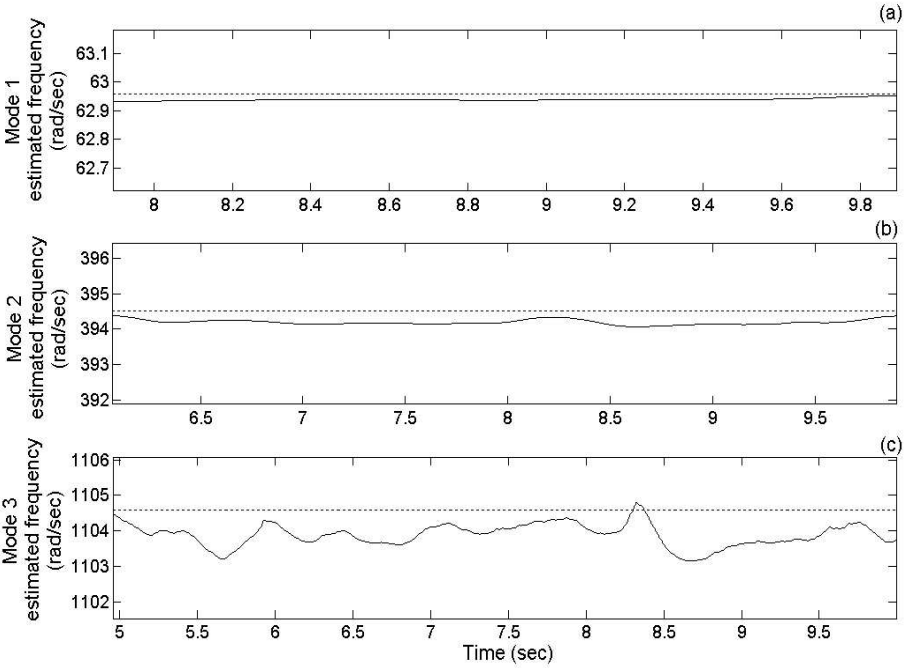
Figure 4.14. Magnified steady-state results for Model 4 estimation.
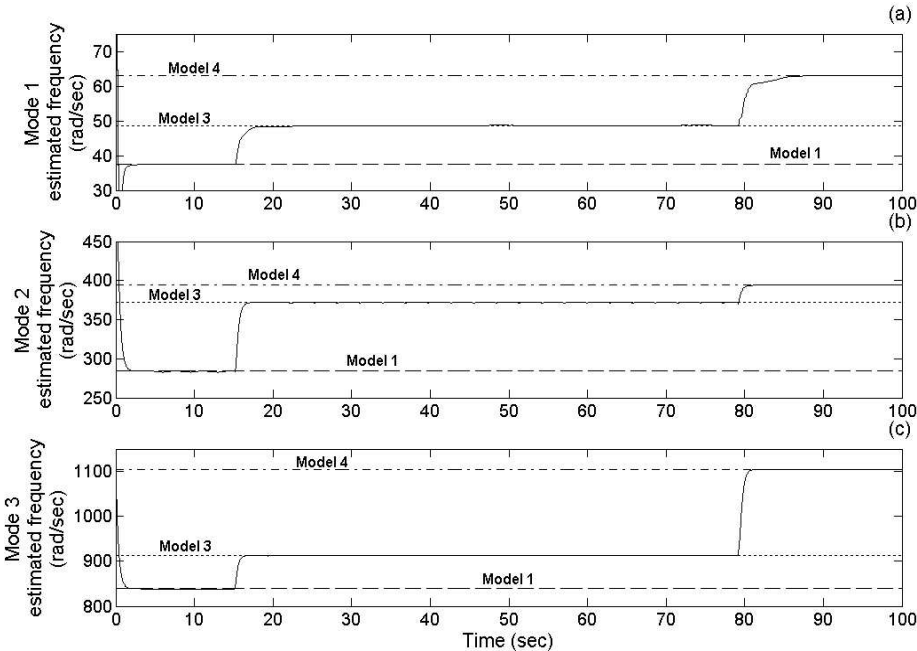
Figure 4.15. Estimation results for the $1 \rightarrow 3 \rightarrow 4$ load sequence.
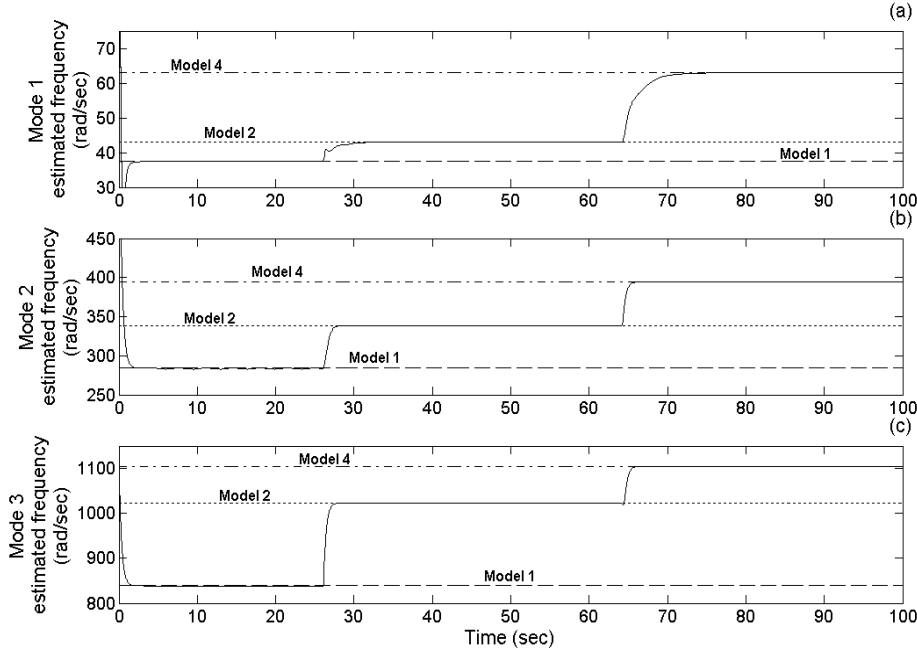

Figure 4.16. Estimation result for the $1 \rightarrow 2 \rightarrow 4$ load sequence.

4.7   Experimental Studies

To test the effectiveness of the proposed estimator in a real-time implementation, and to verify the simulation results given in Section 4.6, experimental studies of the proposed estimator are conducted and described here. The on-line natural frequency estimator is implemented on a dSPACE DS1103 data acquisition and control board using Matlab, Simulink and Real-Time Workshop software. In the implementation, a first-order LPF with low frequency cut-off (2 Hz) is added to the output of each mode estimator. The filters are placed to filter the coefficients a_{1m} and a_{2m} from (4.29) before feeding them to (4.68). The low frequency cut-off is chosen to minimize the fluctuation (i.e., non dc component) in the coefficients a_{1m} and a_{2m}, while retaining the tracking ability of the estimator.

The set-up for this experiment is the same as that employed for the controller implementation described in Chapter 3, with the schematic diagram shown in Fig. 3.34. All the estimators' parameters and the filters' parameters are the same as those used in the simulation in Section 4.6.2. The sampling rate is set at 1 kHz and the beam is excited with white noise. The simulation cases Est.3 and Est.4 are repeated in the experiments.

The experimental results for the estimated frequencies for each mode are shown in Fig. 4.17 for the Est.3 case, and in Fig. 4.18 for the Est.4 case. From the figures, it can be seen that the estimator tracks the changes in the natural frequency of the system as the system changes from one model to the next. The estimated natural frequencies converge to their respective true values between 1 second (for the third mode when the model changes from Model 1 to Model 2) and 3.5 seconds (for the first mode when the model changes from Model 3 to Model 4).

The convergence rate of the estimator used in the experiments is faster than the convergence rate of the same estimator used in the simulations. This is rea-

sonable since in the physical implementation, the estimator receives data input from real plant, which is faster than the simulation model. Moreover, in the physical implementation, the algorithm is embedded in the DSpace board resulting in very fast execution, while in the simulated version the algorithm is executed by a PC processor which also processes other tasks such as calculating and displaying model responses. The convergence rate of the estimator in the physical implementation confirms that the estimator is fast enough to be used in a practical adaptive control system.
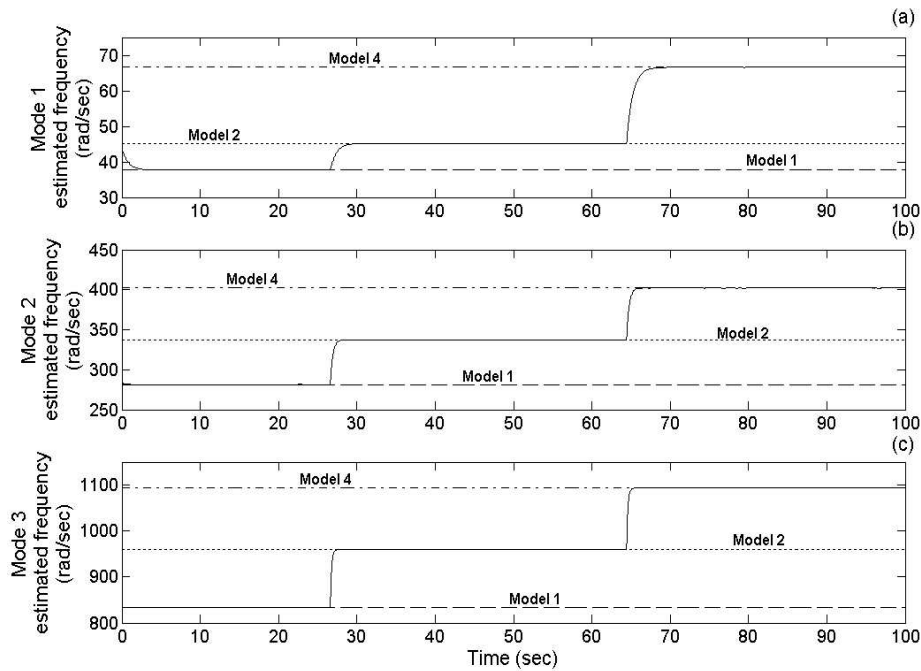
Figure 4.17. Estimation results for the 1 → 3 → 4 load sequence.

To examine the accuracy of the estimator, the magnified outputs of the estimations during steady-state are shown in Figs. 4.19 to 4.22. From the figures, it can be seen that the estimator gives very accurate results with a maximum variance of 0.11% for mode 1 of Model 1.

The physical implementation shows that the proposed estimator is able to give accurate natural frequency estimations for a wide range of frequencies. The
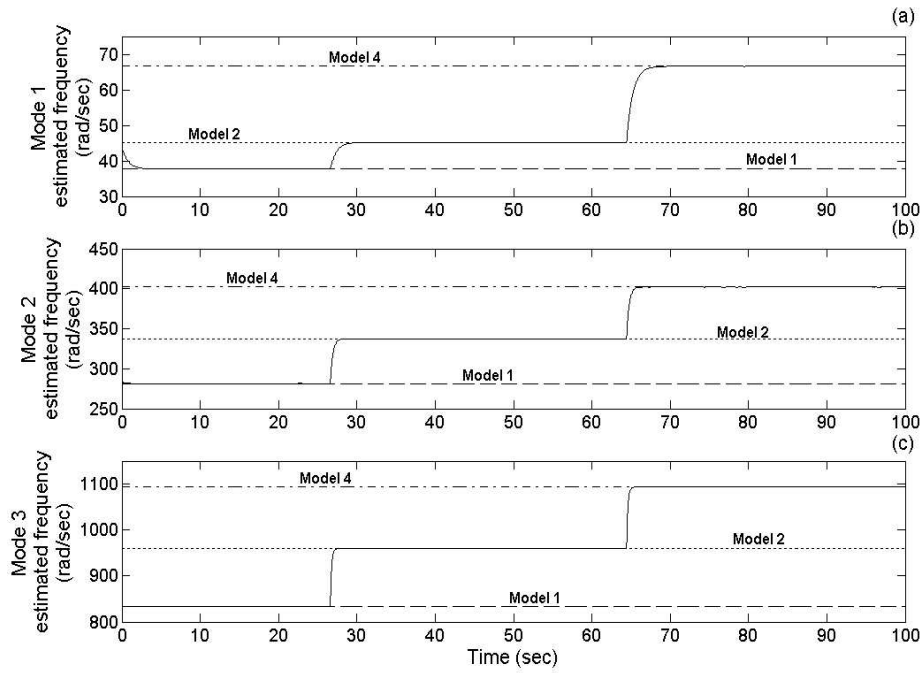
Figure 4.18. Estimation results for the $1 \to 2 \to 4$ load sequence.
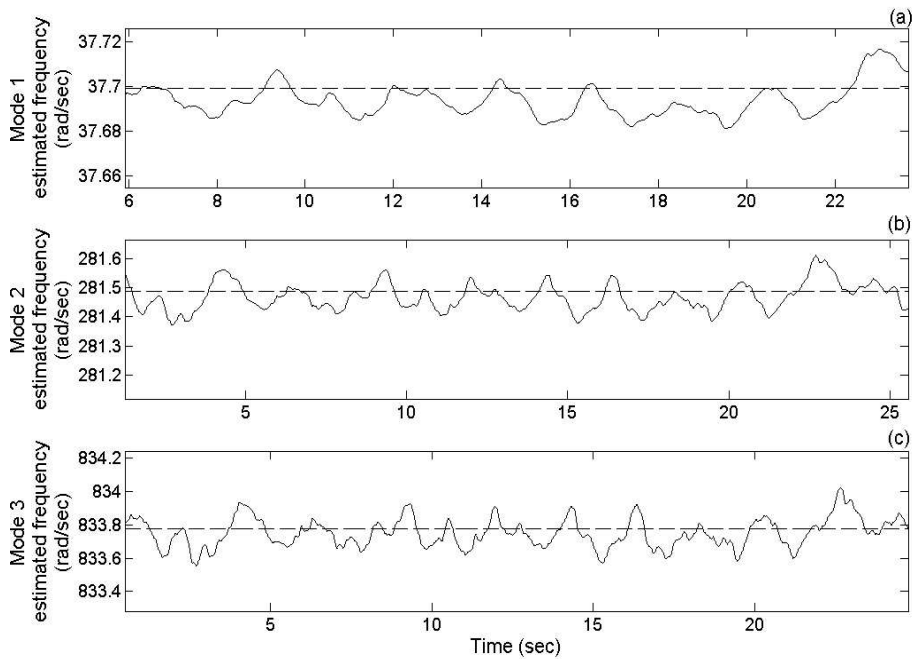

**Figure 4.19. Magnified steady-state results for Model 1 estimation.**
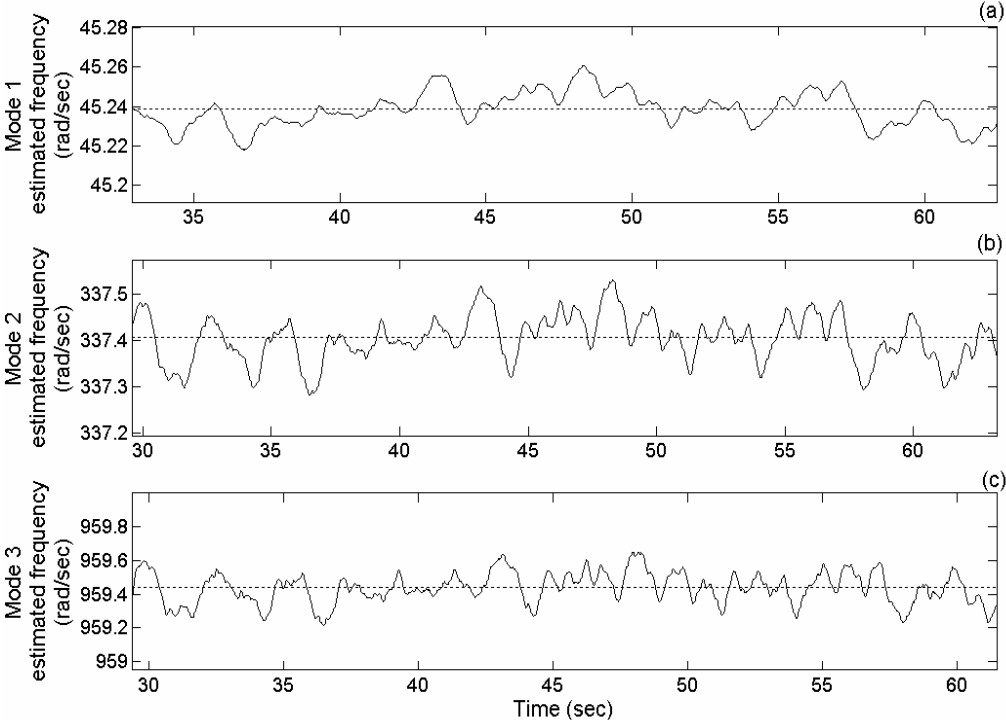
Figure 4.20. Magnified steady-state results for Model 2 estimation.
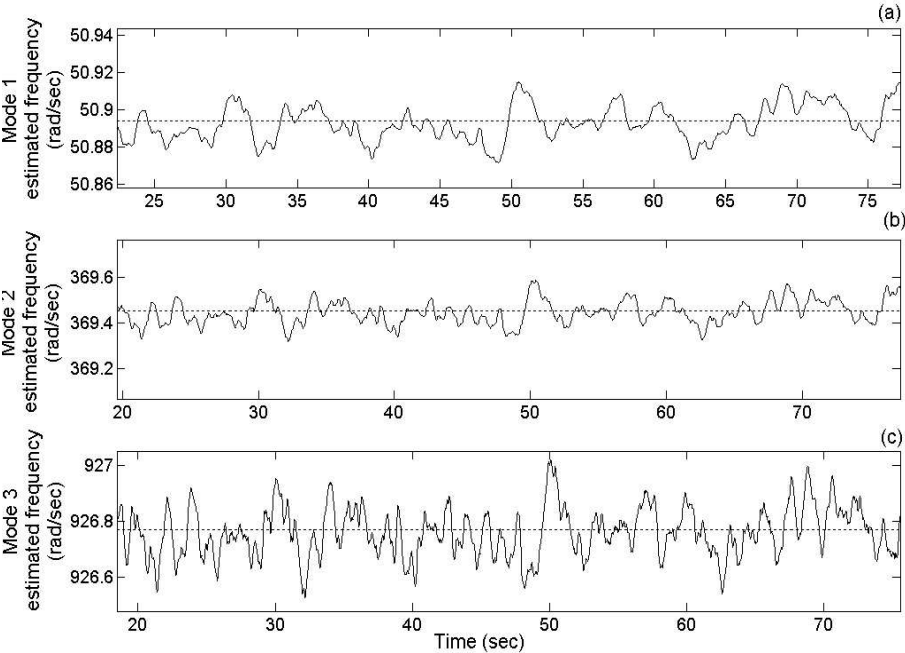
Figure 4.21. Magnified steady-state results for Model 3 estimation.
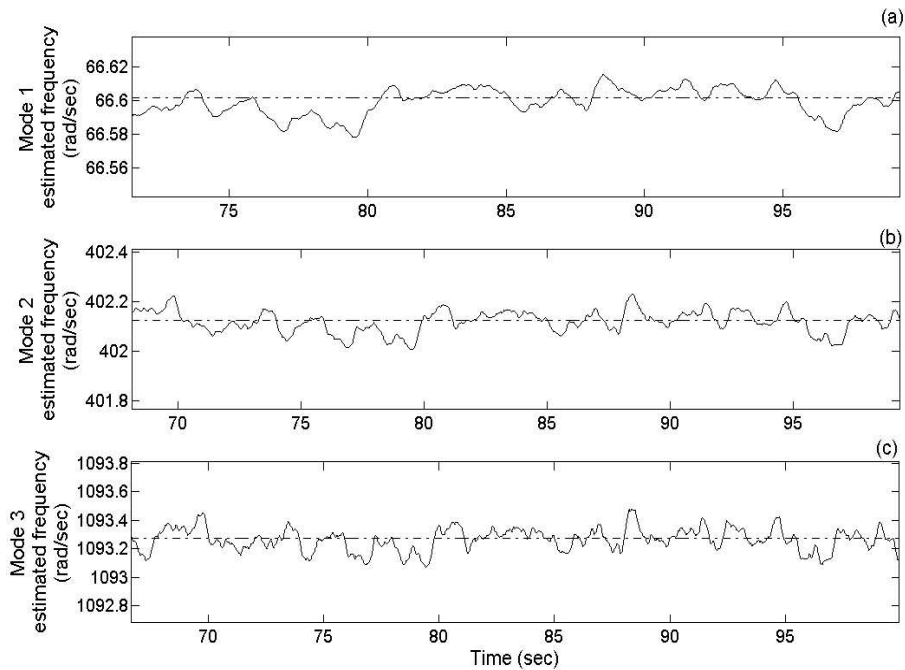
Figure 4.22. Magnified steady-state results for Model 4 estimation.

estimation accuracy of the lowest mode of interest is comparable to the estimation accuracy of the highest mode of interest regardless of the high-pass characteristic of the RLS algorithm employed. It can be concluded from the experimental results that the prefiltering selection and sampling period selection can be designed so as to increase the estimation accuracy of RLS-based estimator. Experimental results reveal that the proposed estimator gives accurate estimations for the first three natural frequencies of the flexible structure. This demonstrates that the proposed natural frequency is able to give accurate results in the presence of unmodeled dynamics due to mode truncation.

4.8 Summary

In this chapter, a real-time natural frequency estimator for flexible structures is proposed. The estimator is designed to perform with high estimation accuracy

for wide-band flexible structures. An analysis of the affect of sampling period and finite word-length on the estimation accuracy reveals that the use of a higher order and a lower sampling period in estimator produces poor estimation results. To achieve high accuracy, therefore, the proposed estimator is built as a set of parallel second-order RLSs with band-pass prefilters and with independent sampling periods for each mode. The parallel structure is constructed using a bank of BPFs, which decomposes the plant into several decoupled second-order systems. This parallel structure enables different sampling periods to be applied independently with different modes. In this way a lower order estimator with a suitable sampling period for each particular mode is obtained. In addition to increasing the estimation accuracy, the parallel structure of the estimator with its own prefiltering for each mode also increases the robustness of the estimator to unmodeled dynamics, and also reduces the computational complexity.

The simulation results and experimental results show that the proposed estimator gives accurate estimation, and the estimator is able to cope with the varying plant parameters and unmodeled dynamics.